Systematic investigation of the high-K isomers and the high-spin rotational bands in the neutron-rich Nd and Sm isotopes by a particle-number conserving method

Zhen-Hua Zhang (张振华)*

Mathematics and Physics Department, North China Electric Power University, Beijing 102206, China

(Received 29 April 2018; revised manuscript received 25 June 2018; published 7 September 2018)

The rotational properties of the neutron-rich Nd and Sm isotopes with mass number $A \approx 150$ are systematically investigated by using the cranked shell model with pairing correlations treated by a particle-number conserving method, in which the Pauli blocking effects are taken into account exactly. The two-quasiparticle states in even-even Nd and Sm isotopes with excitation energies lower than 2.5 MeV are systematically calculated. The available data can be well reproduced and some possible two- and four-quasiparticle isomers are also suggested for future experiments. The experimentally observed rotational frequency variations of moments of inertia for the even-even and odd-A nuclei are reproduced very well by the calculations. The effects of high-order deformation ε_6 on the two-quasiparticle excitation energies and moments of inertia of the ground-state bands in even-even Nd and Sm isotopes are analyzed in detail. By analyzing the occupation probability n_μ of each cranked Nilsson orbitals near the Fermi surface and the contribution of each major shell to the angular-momentum alignments, the alignment mechanism in these nuclei is understood clearly.

DOI: 10.1103/PhysRevC.98.034304

I. INTRODUCTION

For neutron-rich rare-earth nuclei with mass number $A \approx 150$, especially Nd ($Z = 60$) and Sm ($Z = 62$) isotopes, there are many novel phenomena, e.g., nuclear quantum phase transition from spherical to deformed shape [1,2], octupole vibration [3–5], K isomers [6], etc. From the neutron number $N = 92$, the nuclei are well deformed and possess prolate ground-state rotational bands. In this mass region, there are several high-K orbitals around the proton and neutron Fermi surface, e.g., $\pi 5/2^+[413]$, $\pi 5/2^-[532]$, $\pi 7/2^-[523]$, $\nu 5/2^-[523]$, $\nu 5/2^+[642]$, and $\nu 7/2^+[633]$. Therefore, this may give rise to the formation of various high-K multi-quasiparticle (multi-qp) isomers, which are particularly favorable for studying the blocking effects of the pairing correlations.

Due to the high statistics, the spontaneous fission of the actinide nuclei has been used to populate the isomeric and high-spin states of neutron-rich nuclei in the $A \approx 150$ mass region [7–9]. Up to now, using the spontaneous fission of ^{252}Cf [10–19] and in-flight fission of a ^{238}U beam on a ^{9}Be target [20–22], various high-K isomers and high-spin rotational bands for the neutron-rich Nd and Sm isotopes, including both the even-even and the odd-A nuclei, have been established. Most recently, the lightest four-qp high-K isomer in this mass region has been observed in ^{160}Sm [21]. These data can reveal detailed information on the single-particle structure, shell structure, the high-K isomerism, etc., thus providing a benchmark for various nuclear models.

Several nuclear models have been used to investigate the properties of these neutron-rich nuclei, including the quasiparticle rotor model [16,17], a mean-field-type Hartree–Fock–Bogoliubov theory with Gogny force D1S [13], a projected shell model [23,24], and potential-energy-surface calculations [20,21]. However, most of these models focus on the even-even nuclei. Only the projected shell model and the quasiparticle rotor model were used to investigate the odd-A nuclei ^{159}Sm [17,23]. Therefore, it is necessary to perform a systematic investigation including both the even-even and the odd-A Nd and Sm isotopes, which can improve our understanding for these neutron-rich nuclei.

In the present work, the cranked shell model (CSM) with pairing correlations treated by a particle-number conserving (PNC) method [25,26] is used to investigate systematically the neutron-rich Nd and Sm isotopes with mass number $A \approx 150$, including both even-even and odd-A nuclei. In contrast to the conventional Bardeen–Cooper–Schrieffer or Hartree–Fock–Bogoliubov approaches, the many-body Hamiltonian is solved directly in a sufficiently large truncated Fock space in the PNC method [27]. Therefore, the particle number is conserved and the Pauli blocking effects are treated exactly. The PNC-CSM has been employed successfully for describing various phenomena, e.g., the odd-even differences in moments of inertia (MOIs) [28], identical bands [29,30], the nuclear pairing phase transition [31], antimagnetic rotation [32,33], rotational bands and high-K isomers in the rare-earth [34–38] and actinide nuclei [39–42], etc. The PNC scheme has also been used both in relativistic and nonrelativistic mean-field models [43–45] and the total-Routhian-surface method with the Woods–Saxon potential [46,47]. Recently, the PNC method based on the cranking covariant density-functional theory has been developed [48]. Similar approaches to treat pairing correlations with exactly conserved particle number can be found in Refs. [49–54].

This paper is organized as follows: A brief introduction to the PNC treatment of pairing correlations within the CSM

*zhzhang@ncepu.edu.cn

is presented in Sec. II. The numerical details used in PNC calculations are given in Sec. III. In Sec. IV, the two-qp energies and MOIs are calculated and compared with the data. The two-qp states in even-even Nd and Sm isotopes with excitation energies lower than 2.5 MeV are systematically investigated. The effects of high-order deformation ε_6 and alignment mechanism in these nuclei are discussed in detail. A brief summary is given in Sec. V.

II. PARTICLE-NUMBER CONSERVING CRANKED SHELL-MODEL FORMALISM

The cranked shell-model Hamiltonian of an axially symmetric nucleus in the rotating frame can be written as

$$H_{\rm CSM} = H_0 + H_{\rm P} = H_{\rm Nil} - \omega J_x + H_{\rm P}, \tag{1}$$

where $H_{\rm Nil}$ is the Nilsson Hamiltonian [55], and $-\omega J_x$ is the Coriolis interaction with the cranking frequency ω about the x axis (perpendicular to the nuclear symmetry z axis). $H_{\rm P} = H_{\rm P}(0) + H_{\rm P}(2)$ is the pairing interaction,

$$H_{\rm P}(0) = -G_0 \sum_{\xi\eta} a^\dagger_\xi a^\dagger_{\bar\xi} a_{\bar\eta} a_\eta, \tag{2}$$

$$H_{\rm P}(2) = -G_2 \sum_{\xi\eta} q_2(\xi) q_2(\eta) a^\dagger_\xi a^\dagger_{\bar\xi} a_{\bar\eta} a_\eta, \tag{3}$$

where $\bar\xi$ ($\bar\eta$) labels the time-reversed state of a Nilsson state ξ (η), $q_2(\xi) = \sqrt{16\pi/5}\langle\xi|r^2 Y_{20}|\xi\rangle$ is the diagonal element of the stretched quadrupole operator, and G_0 and G_2 are the effective strengths of the monopole and quadrupole pairing interaction, respectively.

Instead of the usual the single-particle-level truncation in conventional shell-model calculations, a cranked many-particle configuration (CMPC) truncation (Fock-space truncation) is adopted, which is crucial to make the PNC calculations for low-lying excited states both workable and sufficiently accurate [27,56]. Usually, a CMPC space with the dimension of 1000 should be enough for the calculations of rare-earth nuclei. By diagonalizing the $H_{\rm CSM}$ in a sufficiently large CMPC space, sufficiently accurate solutions for low-lying excited eigenstates of $H_{\rm CSM}$ can be obtained, which can be written as

$$|\Psi\rangle = \sum_i C_i |i\rangle \ (C_i \text{ real}), \tag{4}$$

where $|i\rangle$ is a CMPC (an eigenstate of the one-body operator H_0).

The angular-momentum alignment for the state $|\Psi\rangle$ is

$$\langle\Psi|J_x|\Psi\rangle = \sum_i C_i^2 \langle i|J_x|i\rangle + 2\sum_{i<j} C_i C_j \langle i|J_x|j\rangle, \tag{5}$$

and the kinematic MOI of state $|\Psi\rangle$ is

$$J^{(1)} = \frac{1}{\omega}\langle\Psi|J_x|\Psi\rangle. \tag{6}$$

Because J_x is a one-body operator, the matrix element $\langle i|J_x|j\rangle$ ($i \neq j$) may not vanish only when $|i\rangle$ and $|j\rangle$ differ by one particle occupation [26]. After a certain permutation of creation operators, $|i\rangle$ and $|j\rangle$ can be recast into

$$|i\rangle = (-1)^{M_{i\mu}}|\mu\cdots\rangle, \quad |j\rangle = (-1)^{M_{j\nu}}|\nu\cdots\rangle, \tag{7}$$

where μ and ν denote two different single-particle states, and $(-1)^{M_{i\mu}} = \pm 1$, $(-1)^{M_{j\nu}} = \pm 1$ according to whether the permutation is even or odd. Therefore, the angular-momentum alignment of $|\Psi\rangle$ can be expressed as

$$\langle\Psi|J_x|\Psi\rangle = \sum_\mu j_x(\mu) + \sum_{\mu<\nu} j_x(\mu\nu). \tag{8}$$

where the diagonal contribution $j_x(\mu)$ and the off-diagonal (interference) contribution $j_x(\mu\nu)$ can be written as

$$j_x(\mu) = \langle\mu|j_x|\mu\rangle n_\mu, \tag{9}$$

$$j_x(\mu\nu) = 2\langle\mu|j_x|\nu\rangle \sum_{i<j} (-1)^{M_{i\mu}+M_{j\nu}} C_i C_j \ (\mu \neq \nu), \tag{10}$$

and

$$n_\mu = \sum_i |C_i|^2 P_{i\mu} \tag{11}$$

is the occupation probability of the cranked orbital $|\mu\rangle$, $P_{i\mu} = 1$ if $|\mu\rangle$ is occupied in $|i\rangle$, and $P_{i\mu} = 0$ otherwise.

III. NUMERICAL DETAILS

In this work, the deformation parameters (ε_2, ε_4, and ε_6) of Nd and Sm isotopes used in PNC-CSM calculations are taken from Ref. [57], which are shown at Table I. The Nilsson parameters (κ and μ) are assigned the traditional values [55]. The experimental data show that the ground state of the $N = 93$ isotones (e.g., ^{153}Nd and ^{155}Sm) is $\nu 3/2^-[521]$ [58,59].

TABLE I. Deformation parameters (ε_2, ε_4, and ε_6) of Nd and Sm isotopes used in present PNC-CSM calculations, which are taken from Ref. [57].

	^{152}Nd	^{153}Nd	^{154}Nd	^{155}Nd	^{156}Nd	^{157}Nd	^{158}Nd	^{159}Nd	^{160}Nd
ε_2	0.242	0.250	0.250	0.258	0.258	0.258	0.258	0.258	0.267
ε_4	−0.080	−0.073	−0.067	−0.060	−0.053	−0.047	−0.040	−0.033	−0.027
ε_6	0.026	0.031	0.034	0.037	0.038	0.040	0.040	0.042	0.043
	^{154}Sm	^{155}Sm	^{156}Sm	^{157}Sm	^{158}Sm	^{159}Sm	^{160}Sm	^{161}Sm	^{162}Sm
ε_2	0.250	0.250	0.258	0.258	0.258	0.267	0.267	0.275	0.275
ε_4	−0.067	−0.060	−0.053	−0.047	−0.040	−0.033	−0.027	−0.013	−0.007
ε_6	0.030	0.032	0.038	0.038	0.040	0.044	0.044	0.045	0.046

However, the calculated ground state using the traditional Nilsson parameters is $\nu 5/2^+[642]$ [55]. Therefore, to reproduce the experimental level sequence, the neutron orbital $\nu 5/2^+[642]$ is shifted upwards slightly by $0.07\hbar\omega_0$ for all these nuclei.

The effective pairing strengths for each nuclei, in principle, can be determined by the experimental odd-even differences in nuclear binding energies [60],

$$\begin{aligned} P_{\rm p} &= \tfrac{1}{2}[B(Z+1,N)+B(Z-1,N)]-B(Z,N) \\ &= E_{\rm g}(Z,N)-\tfrac{1}{2}[E_{\rm g}(Z+1,N)+E_{\rm g}(Z-1,N)], \\ P_{\rm n} &= \tfrac{1}{2}[B(Z,N+1)+B(Z,N-1)]-B(Z,N) \\ &= E_{\rm g}(Z,N)-\tfrac{1}{2}[E_{\rm g}(Z,N+1)+E_{\rm g}(Z,N-1)], \quad (12) \end{aligned}$$

where $E_{\rm g}$ is the ground-state energy of the nucleus and is connected with the dimension of the truncated CMPC space. In this work, the CMPC space is constructed in the proton $N=4$, 5 major shells and the neutron $N=5$, 6 major shells, respectively. The CMPC truncation energies are about $0.85\hbar\omega_0$ for protons and $0.80\hbar\omega_0$ for neutrons, respectively. The dimensions of the CMPC space are about 1000 for both protons and neutrons in the present calculation. For all Nd and Sm isotopes, the corresponding effective monopole and quadrupole pairing strengths are chosen as $G_{0\rm p}=0.25$ MeV and $G_{2\rm p}=0.01$ MeV fm^{-4} for protons, $G_{0\rm n}=0.30$ MeV and $G_{2\rm n}=0.02$ MeV fm^{-4} for neutrons. Figure 1 shows the comparison between experimental (black solid circles) and calculated (red open circles) neutron odd-even difference P_n for Nd (upper panel) and Sm (lower panel) isotopes. It can be seen that the data can be well reproduced. In principal, the pairing strengths should be different for each nucleus. Note that, for some neutron-rich Nd and Sm nuclei, the experimental binding energy is not accurate [60]. Therefore, in the present work the pairing strengths for all nuclei are chosen as the same value to get a global fit.

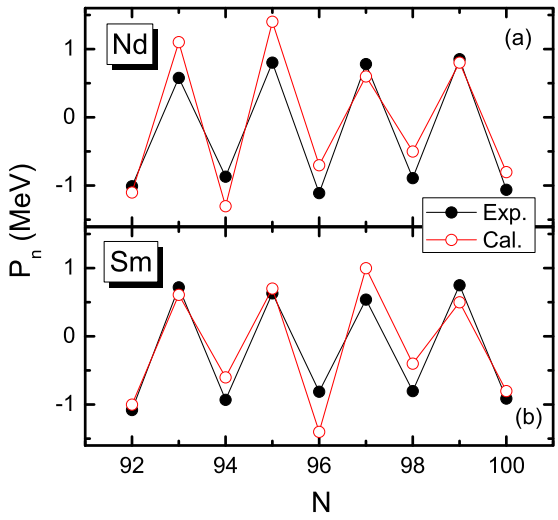

FIG. 1. Comparison between the experimental (black solid circles) and calculated (red open circles) neutron odd-even difference P_n for Nd (upper panel) and Sm (lower panel) isotopes. The experimental binding energies are taken from Ref. [60].

Previous investigations have shown that, after the quadrupole pairing being included, the description of the experimental bandhead energies and the level crossing frequencies can be improved [61]. As for the quadrupole pairing, the strength is determined by the bandhead MOIs in the present work. The quadrupole pairing is also included in the projected shell model when investigating the Nd and Sm isotopes, in which BCS method is used to treat the pairing correlations [23]. In the projected shell model, the quadrupole pairing strength is chosen to be proportional to the monopole pairing strength with proportionality constant 0.18 [23]. As for this point, this proportionality is much smaller in the present work (less than 0.1). However, the PNC method is different from the BCS method. Therefore, the effective pairing strength should be different.

The stability of the calculations against the change of the dimension of the CMPC space has been investigated in Refs. [26,41,56]. In the present calculations, almost all of the CMPCs with weight >0.1% in the many-body wave functions are taken into account, so the solutions to the low-lying excited states are accurate enough. A larger CMPC space with renormalized pairing strengths gives essentially the same results.

IV. RESULTS AND DISCUSSION

A. Cranked Nilsson levels

As an example of Nd and Sm isotopes around the $A\approx 150$ mass region, the calculated cranked Nilsson levels near the Fermi surface of ^{156}Sm are shown in Fig. 2. The positive (negative) parity levels are denoted by blue (red) lines. The signature $\alpha=+1/2$ ($\alpha=-1/2$) levels are denoted by solid (dotted) lines. It can be seen from Fig. 2 that there are several

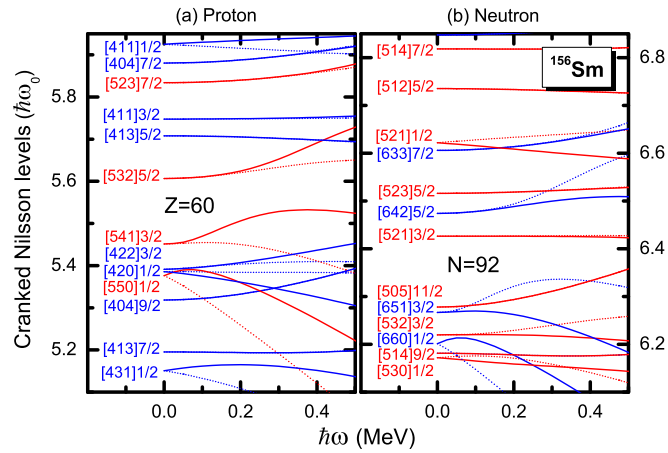

FIG. 2. The cranked Nilsson levels near the Fermi surface of ^{156}Sm for (a) protons and (b) neutrons. The positive (negative) parity levels are denoted by blue (red) lines. The signature $\alpha=+1/2$ ($\alpha=-1/2$) levels are denoted by solid (dotted) lines. The Nilsson parameters (κ and μ) are taken as the traditional values [55]. The deformation parameters $\varepsilon_2=0.258$, $\varepsilon_4=-0.053$, and $\varepsilon_6=0.038$ are taken from Ref. [57]. In addition, the neutron orbital $\nu 5/2^+[642]$ is shifted upwards slightly by $0.07\hbar\omega_0$ to reproduce the experimental level sequence.

TABLE II. two-qp states in even-even Nd isotopes calculated by PNC-CSM with ($E_{\rm cal}$) and without ($E^*_{\rm cal}$) ε_6 deformation, where $|\Delta E| = |E_{\rm cal} - E^*_{\rm cal}|$. The data are taken from Refs. [16,22].

Nucleus	K^π	Configuration	$E_{\rm exp}$ (keV)	$E_{\rm cal}$ (keV)	$E^*_{\rm cal}$ (keV)	$\lvert\Delta E\rvert$
^{152}Nd	4^+	$\pi^2\frac{3}{2}^-[541]\otimes\frac{5}{2}^-[532]$		2038	2177	139
^{152}Nd	4^-	$\pi^2\frac{3}{2}^+[422]\otimes\frac{5}{2}^-[532]$		2107	2148	41
^{152}Nd	3^-	$\pi^2\frac{1}{2}^+[420]\otimes\frac{5}{2}^-[532]$		2325	2398	73
^{154}Nd	4^-	$\nu^2\frac{3}{2}^-[521]\otimes\frac{5}{2}^+[642]$	1298 [16]	1263	1307	44
^{154}Nd	4^+	$\nu^2\frac{3}{2}^-[521]\otimes\frac{5}{2}^-[523]$		1575	1550	25
^{154}Nd	5^-	$\nu^2\frac{5}{2}^-[523]\otimes\frac{5}{2}^+[642]$		1921	2026	105
^{154}Nd	5^-	$\nu^2\frac{3}{2}^-[521]\otimes\frac{7}{2}^+[633]$		2333	2396	63
^{154}Nd	2^+	$\nu^2\frac{1}{2}^-[521]\otimes\frac{3}{2}^-[521]$		2400	2346	54
^{154}Nd	4^+	$\pi^2\frac{3}{2}^-[541]\otimes\frac{5}{2}^-[532]$		1906	2090	184
^{154}Nd	4^-	$\pi^2\frac{3}{2}^+[422]\otimes\frac{5}{2}^-[532]$		2085	2127	42
^{154}Nd	3^-	$\pi^2\frac{1}{2}^+[420]\otimes\frac{5}{2}^-[532]$		2222	2310	88
^{156}Nd	5^-	$\nu^2\frac{5}{2}^-[523]\otimes\frac{5}{2}^+[642]$	1431 [16]	1437	1351	86
^{156}Nd	4^+	$\nu^2\frac{3}{2}^-[521]\otimes\frac{5}{2}^-[523]$		1501	1555	54
^{156}Nd	6^+	$\nu^2\frac{5}{2}^+[642]\otimes\frac{7}{2}^+[633]$		2075	2152	77
^{156}Nd	4^-	$\nu^2\frac{3}{2}^-[521]\otimes\frac{5}{2}^+[642]$		2086	1970	116
^{156}Nd	5^-	$\nu^2\frac{3}{2}^-[521]\otimes\frac{7}{2}^+[633]$		2179	2341	162
^{156}Nd	3^-	$\nu^2\frac{1}{2}^-[521]\otimes\frac{5}{2}^+[642]$		2204	2143	61
^{156}Nd	6^-	$\nu^2\frac{5}{2}^-[523]\otimes\frac{7}{2}^+[633]$		2292	2295	3
^{156}Nd	2^+	$\nu^2\frac{1}{2}^-[521]\otimes\frac{3}{2}^-[521]$		2378	2285	93
^{156}Nd	4^+	$\pi^2\frac{3}{2}^-[541]\otimes\frac{5}{2}^-[532]$		1863	1983	120
^{156}Nd	4^-	$\pi^2\frac{3}{2}^+[422]\otimes\frac{5}{2}^-[532]$		2130	2096	34
^{156}Nd	3^-	$\pi^2\frac{1}{2}^+[420]\otimes\frac{5}{2}^-[532]$		2188	2224	36
^{158}Nd	6^-	$\nu^2\frac{5}{2}^-[523]\otimes\frac{7}{2}^+[633]$	1648 [22]	1557	1595	38
^{158}Nd	3^+	$\nu^2\frac{1}{2}^-[521]\otimes\frac{5}{2}^-[523]$		1745	1632	113
^{158}Nd	6^+	$\nu^2\frac{5}{2}^+[642]\otimes\frac{7}{2}^+[633]$		2104	2004	100
^{158}Nd	5^-	$\nu^2\frac{3}{2}^-[521]\otimes\frac{7}{2}^+[633]$		2263	2275	12
^{158}Nd	3^-	$\nu^2\frac{1}{2}^-[521]\otimes\frac{5}{2}^+[642]$		2283	2039	244
^{158}Nd	2^+	$\nu^2\frac{1}{2}^-[521]\otimes\frac{3}{2}^-[521]$		2442	2309	133
^{158}Nd	4^+	$\pi^2\frac{3}{2}^-[541]\otimes\frac{5}{2}^-[532]$		1699	1862	163
^{158}Nd	3^-	$\pi^2\frac{1}{2}^+[420]\otimes\frac{5}{2}^-[532]$		2077	2158	81
^{158}Nd	4^-	$\pi^2\frac{3}{2}^+[422]\otimes\frac{5}{2}^-[532]$		2097	2105	8
^{158}Nd	4^-	$\pi^2\frac{5}{2}^+[413]\otimes\frac{3}{2}^-[541]$		2381	2173	208
^{160}Nd	4^-	$\nu^2\frac{1}{2}^-[521]\otimes\frac{7}{2}^+[633]$	1108 [22]	1243	1258	15
^{160}Nd	3^+	$\nu^2\frac{1}{2}^-[521]\otimes\frac{5}{2}^-[523]$		1845	1991	146
^{160}Nd	6^-	$\nu^2\frac{5}{2}^-[523]\otimes\frac{7}{2}^+[633]$		2117	2037	80
^{160}Nd	6^-	$\nu^2\frac{5}{2}^-[512]\otimes\frac{7}{2}^+[633]$		2215	1941	274
^{160}Nd	3^-	$\nu^2\frac{1}{2}^-[521]\otimes\frac{5}{2}^+[642]$		2412	2435	23
^{160}Nd	3^+	$\nu^2\frac{1}{2}^-[521]\otimes\frac{5}{2}^-[512]$		2451	2012	439
^{160}Nd	4^+	$\pi^2\frac{3}{2}^-[541]\otimes\frac{5}{2}^-[532]$		1656	1797	141
^{160}Nd	3^-	$\pi^2\frac{1}{2}^+[420]\otimes\frac{5}{2}^-[532]$		2033	2111	78
^{160}Nd	4^-	$\pi^2\frac{3}{2}^+[422]\otimes\frac{5}{2}^-[532]$		2127	2126	1
^{160}Nd	7^-	$\pi^2\frac{9}{2}^+[404]\otimes\frac{5}{2}^-[532]$		2336	2516	180

high-K orbitals around the proton and neutron Fermi surface, e.g., $\pi 5/2^+[413]$, $\pi 5/2^-[532]$, $\pi 7/2^-[523]$, $\nu 5/2^-[523]$, $\nu 5/2^+[642]$, and $\nu 7/2^+[633]$. Therefore, this may lead to the formation of various high-K multi-qp isomers in Nd and Sm isotopes around $A \approx 150$ mass region. It also can be seen that there are two subshells at proton number $Z = 60$ and neutron number $N = 92$, respectively. So for Nd ($Z = 60$) isotopes, the excitation energies of the proton two-qp states should

be a little higher. The experimentally favored two-qp states should be based on neutron configurations. Indeed, no proton two-qp state in neutron-rich Nd isotopes has been observed experimentally up to now. The energy gap at $Z = 62$ is much smaller than that of $Z = 60$. So for Sm ($Z = 62$) isotopes, the proton two-qp states should exist.

B. Two-quasiparticle excitation energies in even-even Nd and Sm isotopes

A series of two-qp isomers have been observed experimentally in even-even Nd and Sm isotopes at the $A \approx 150$ mass region [16,19–22] which provide detailed information for these neutron-rich nuclei. It should be noted that, in this mass region, the high-order deformation ε_6 is remarkable [57] and has a measurable effect on the structure of these nuclei, e.g., the inclusion of ε_6 will alter the the two-qp excitation energy by about 250 keV [20]. Systematically calculated two-qp states in even-even Nd isotopes with excitation energies lower than 2.5 MeV are shown in Table II. $E_{\rm cal}$ and $E^*_{\rm cal}$ denote the calculated results with and without ε_6 deformation, respectively. In addition, the energy differences $|\Delta E| = |E_{\rm cal} - E^*_{\rm cal}|$ are also shown in the last column. It can be seen that the data are reproduced quite well by the PNC-CSM calculations no matter whether the ε_6 deformation is considered or not. This indicates that the adopted single-particle level scheme is suitable for the PNC-CSM calculations. The energy differences $|\Delta E|$ for these four observed two-qp states are all less than 100 keV. It seems that the ε_6 deformation has small effects on the excitation energies of these two-qp states. However, if one see through Table II, the effects of ε_6 deformation are prominent in some two-qp states. For example, the excitation energy of the 3^+ state with configuration $\nu^2 1/2^-[521] \otimes 5/2^-[512]$ in ^{160}Nd is lowered by 439 keV after the ε_6 deformation is neglected. This is because, after the ε_6 deformation is switched off, the sequence of the single-particle levels is changed. The root-mean-square deviation between $E_{\rm cal}$ and $E^*_{\rm cal}$ is about 130 keV. Therefore, the ε_6 deformation still has remarkable effects on the excitation energies of the two-qp states. Due to the large shell gap at $Z = 60$, the energies of the proton two-qp states in Nd isotopes are all quite high. However, with increasing neutron number, the energy of the lowest proton two-qp state with $K^\pi = 4^+$ in each Nd isotope decreases from more than 2.0 MeV to about 1.6 MeV, which may be observed in future experiments. The lowering of the excitation energy of the $K^\pi = 4^+$ state is caused by the decreasing of the $Z = 60$ shell gap with increasing neutron number. Since the proton-neutron residual interaction is neglected in the PNC-CSM calculations, the excitation energies of the four-qp states with two quasi-protons and two quasi-neutrons can be simply obtained by summing the energies of the corresponding two-qp states. Especially for ^{160}Nd, the excitation energy of the four-qp state $K^\pi = 8^-$ ($\pi^2 3/2^-[541]5/2^-[532] \otimes \nu^2 1/2^-[521]7/2^+[633]$) is only about 2899 keV from the PNC-CSM calculation. Therefore, I hope this state can be observed by future experiments.

In Table III, similar results are shown for Sm isotopes. Different from Nd isotopes, the shell gap at $Z = 62$ is much smaller, so the proton two-qp states should exist. Indeed, two-qp states with $K^\pi = 5^-$ based on proton configuration $\pi^2 5/2^+[413] \otimes 5/2^-[532]$ have been observed in ^{158}Sm [19] and ^{160}Sm [21]. The available data are also reproduced quite well by the PNC-CSM calculations, especially after considering the ε_6 deformation. From Table III it can be seen that the effects of ε_6 deformation on Sm isotopes are more prominent than Nd isotopes. The root-mean-square deviation between $E_{\rm cal}$ and $E^*_{\rm cal}$ is about 260 keV, which is consistent with the potential-energy-surface calculations in Ref. [20]. In Ref. [16], the calculated lowest two-qp state in ^{156}Sm using the quasiparticle rotor model is $K^\pi = 4^-$. However, in their calculation, the $K^\pi = 5^-$ state is yrast with increasing spin. Therefore, they assigned the 1398 keV state in ^{156}Sm as $K^\pi = 5^-$. In the PNC-CSM calculations, the excitation energy for $K^\pi = 5^-$ is much higher than 1398 keV, whereas that calculated for $K^\pi = 4^-$ is very close to the data. In addition, the excitation energies of the two $K^\pi = 5^-$ states in ^{158}Sm are quite close to each other, so their configurations need further investigation. These will be discussed later. Recently, one four-qp isomer with excitation energy 2757 keV has been observed in ^{160}Sm, which is assigned as $K^\pi = 11^-$ ($\pi^2 5/2^+[413]5/2^-[532] \otimes \nu^2 5/2^-[523]7/2^+[633]$). It can be seen that the proton two-qp state $\pi^2 5/2^+[413]5/2^-[532]$ and neutron two-qp state $\nu^2 5/2^-[523]7/2^+[633]$ are all the lowest-lying two-qp excitations in ^{160}Sm. The calculated excitation energy for this four-qp state is 2918 keV, which is very close to the data. Due to the low excitation energy of the proton two-qp states in Sm isotopes, possible four-qp states with the lowest two-quasi-proton and two-quasi-neutron configurations may exist.

C. Rotational properties in Nd and Sm isotopes

Furthermore, the rotational bands observed in Nd and Sm isotopes are analyzed. Figure 3 shows the experimental (solid circles) and calculated (solid black lines) kinematic MOIs $J^{(1)}$ for the ground-state bands (GSBs) in even-even Nd (upper panel) and Sm (lower panel) isotopes from $N = 92$ to $N = 100$. The calculated results without high-order deformation ε_6 are also shown as red lines. The experimental kinematic MOIs for each band are extracted by

$$\frac{J^{(1)}(I)}{\hbar^2} = \frac{2I+1}{E_\gamma(I+1 \to I-1)} \tag{13}$$

separately for each signature sequence within a rotational band ($\alpha = I \mod 2$). The relation between the rotational frequency ω and nuclear angular momentum I is

$$\hbar\omega(I) = \frac{E_\gamma(I+1 \to I-1)}{I_x(I+1) - I_x(I-1)}, \tag{14}$$

where $I_x(I) = [(I+1/2)^2 - K^2]^{1/2}$, K is the projection of nuclear total angular momentum along the symmetry z axis of an axially symmetric nuclei. It can be seen that the MOIs and their variations with the rotational frequency are well reproduced by the PNC-CSM calculations. The data show that there is no sharp upbending in all Nd and Sm isotopes, which is consistent with the PNC-CSM calculations except for ^{154}Nd and ^{156}Sm. It can be seen that obvious upbendings exist in the calculated MOIs of ^{154}Nd and ^{156}Sm when ε_6

TABLE III. Similar to Table II, but for even-even Sm isotopes. The data are taken from Refs. [16,19,21]. The 1398 keV state in ^{156}Sm was assigned as $K^\pi = 5^-$ in Ref. [16].

Nucleus	K^π	Configuration	$E_{\rm exp}$ (keV)	$E_{\rm cal}$ (keV)	$E^*_{\rm cal}$ (keV)	$\lvert\Delta E\rvert$
^{154}Sm	5^-	$\pi^2\frac{5}{2}^+[413]\otimes\frac{5}{2}^-[532]$		1400	1182	218
^{154}Sm	4^-	$\pi^2\frac{3}{2}^+[411]\otimes\frac{5}{2}^-[532]$		1664	1455	209
^{154}Sm	4^+	$\pi^2\frac{3}{2}^+[411]\otimes\frac{5}{2}^+[413]$		2331	1834	497
^{154}Sm	6^+	$\pi^2\frac{5}{2}^-[532]\otimes\frac{7}{2}^-[523]$		2372	2337	35
^{154}Sm	6^-	$\pi^2\frac{7}{2}^+[404]\otimes\frac{5}{2}^-[532]$		2475	2369	106
^{156}Sm	4^-	$\nu^2\frac{3}{2}^-[521]\otimes\frac{5}{2}^+[642]$	(1398) [16]	1386	1354	32
^{156}Sm	4^+	$\nu^2\frac{3}{2}^-[521]\otimes\frac{5}{2}^-[523]$		1642	1527	115
^{156}Sm	5^-	$\nu^2\frac{5}{2}^-[523]\otimes\frac{5}{2}^+[642]$		1981	2040	59
^{156}Sm	5^-	$\nu^2\frac{3}{2}^-[521]\otimes\frac{7}{2}^+[633]$		2335	2326	9
^{156}Sm	2^+	$\nu^2\frac{1}{2}^-[521]\otimes\frac{3}{2}^-[521]$		2467	2319	148
^{156}Sm	5^-	$\pi^2\frac{5}{2}^+[413]\otimes\frac{5}{2}^-[532]$		1444	1200	244
^{156}Sm	4^-	$\pi^2\frac{3}{2}^+[411]\otimes\frac{5}{2}^-[532]$		1699	1481	218
^{156}Sm	6^+	$\pi^2\frac{5}{2}^-[532]\otimes\frac{7}{2}^-[523]$		2344	2308	36
^{156}Sm	4^+	$\pi^2\frac{3}{2}^+[411]\otimes\frac{5}{2}^+[413]$		2408	1855	553
^{158}Sm	5^-	$\nu^2\frac{5}{2}^-[523]\otimes\frac{5}{2}^+[642]$	1279 [16]	1394	1305	89
^{158}Sm	4^+	$\nu^2\frac{3}{2}^-[521]\otimes\frac{5}{2}^-[523]$		1508	1571	63
^{158}Sm	6^+	$\nu^2\frac{5}{2}^+[642]\otimes\frac{7}{2}^+[633]$		2015	2103	88
^{158}Sm	4^-	$\nu^2\frac{3}{2}^-[521]\otimes\frac{5}{2}^+[642]$		2005	1887	118
^{158}Sm	6^-	$\nu^2\frac{5}{2}^-[523]\otimes\frac{7}{2}^+[633]$		2142	2144	2
^{158}Sm	5^-	$\nu^2\frac{3}{2}^-[521]\otimes\frac{7}{2}^+[633]$		2147	2344	197
^{158}Sm	3^-	$\nu^2\frac{1}{2}^-[521]\otimes\frac{5}{2}^+[642]$		2205	2134	71
^{158}Sm	3^+	$\nu^2\frac{1}{2}^-[521]\otimes\frac{5}{2}^-[523]$		2332	2180	152
^{158}Sm	2^+	$\nu^2\frac{1}{2}^-[521]\otimes\frac{3}{2}^-[521]$		2347	2378	31
^{158}Sm	5^-	$\pi^2\frac{5}{2}^+[413]\otimes\frac{5}{2}^-[532]$	1322 [19]	1384	1197	187
^{158}Sm	4^-	$\pi^2\frac{3}{2}^+[411]\otimes\frac{5}{2}^-[532]$		1665	1472	193
^{158}Sm	6^+	$\pi^2\frac{5}{2}^-[532]\otimes\frac{7}{2}^-[523]$		2279	2272	7
^{158}Sm	4^+	$\pi^2\frac{3}{2}^+[411]\otimes\frac{5}{2}^+[413]$		2329	1762	567
^{160}Sm	6^-	$\nu^2\frac{5}{2}^-[523]\otimes\frac{7}{2}^+[633]$	1468 [21]	1457	1730	273
^{160}Sm	3^+	$\nu^2\frac{1}{2}^-[521]\otimes\frac{5}{2}^-[523]$		1697	1840	143
^{160}Sm	6^+	$\nu^2\frac{5}{2}^+[642]\otimes\frac{7}{2}^+[633]$		2062	2150	88
^{160}Sm	5^-	$\nu^2\frac{3}{2}^-[521]\otimes\frac{7}{2}^+[633]$		2192	2376	184
^{160}Sm	3^-	$\nu^2\frac{1}{2}^-[521]\otimes\frac{5}{2}^+[642]$		2216	2220	4
^{160}Sm	2^+	$\nu^2\frac{1}{2}^-[521]\otimes\frac{3}{2}^-[521]$		2474	2447	27
^{160}Sm	5^-	$\pi^2\frac{5}{2}^+[413]\otimes\frac{5}{2}^-[532]$	1361 [21]	1461	1159	302
^{160}Sm	4^-	$\pi^2\frac{3}{2}^+[411]\otimes\frac{5}{2}^-[532]$		1726	1451	275
^{160}Sm	6^+	$\pi^2\frac{5}{2}^-[532]\otimes\frac{7}{2}^-[523]$		2283	2239	44
^{160}Sm	4^+	$\pi^2\frac{3}{2}^+[411]\otimes\frac{5}{2}^+[413]$		2449	1772	677
^{162}Sm	4^-	$\nu^2\frac{1}{2}^-[521]\otimes\frac{7}{2}^+[633]$		1342	1243	99
^{162}Sm	3^+	$\nu^2\frac{1}{2}^-[521]\otimes\frac{5}{2}^-[523]$		1906	2015	109
^{162}Sm	6^-	$\nu^2\frac{5}{2}^-[512]\otimes\frac{7}{2}^+[633]$		2201	1827	374
^{162}Sm	6^-	$\nu^2\frac{5}{2}^-[523]\otimes\frac{7}{2}^+[633]$		2281	2131	150
^{162}Sm	3^-	$\nu^2\frac{1}{2}^-[521]\otimes\frac{5}{2}^+[642]$		2396	2331	65
^{162}Sm	3^+	$\nu^2\frac{1}{2}^-[521]\otimes\frac{5}{2}^-[512]$		2496	1957	539
^{162}Sm	5^-	$\pi^2\frac{5}{2}^+[413]\otimes\frac{5}{2}^-[532]$		1459	1128	331
^{162}Sm	4^-	$\pi^2\frac{3}{2}^+[411]\otimes\frac{5}{2}^-[532]$		1778	1444	334
^{162}Sm	6^+	$\pi^2\frac{5}{2}^-[532]\otimes\frac{7}{2}^-[523]$		2211	2127	84
^{162}Sm	4^+	$\pi^2\frac{3}{2}^+[411]\otimes\frac{5}{2}^+[413]$		2464	1741	723

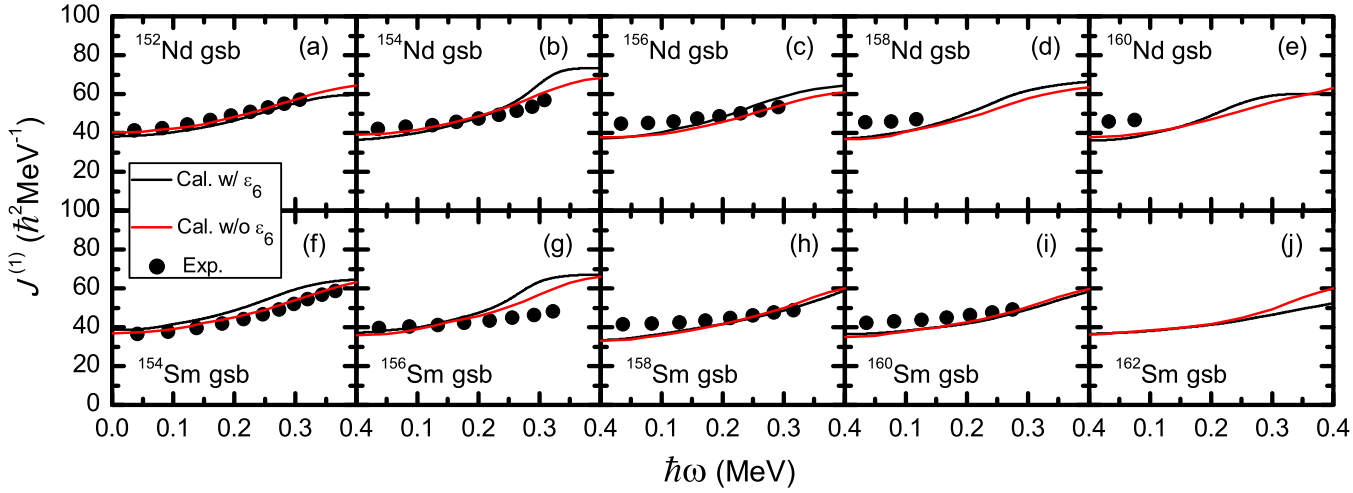

FIG. 3. Experimental (solid circles) and calculated (solid black lines) kinematic MOIs $J^{(1)}$ for the GSBs in even-even Nd and Sm isotopes from $N = 92$ to $N = 100$. The data are taken from Refs. [12,16,22]. The calculated results without high-order deformation ε_6 are also shown as red lines.

deformation is considered. After the ε_6 deformation being switched off, the upbendings become less prominent and the results are more consistent with the data. This indicates that, with the rotational frequency increasing, the ε_6 deformation may become smaller. It also can be seen that, in the low-rotational-frequency region, ε_6 deformation has little effect on the MOIs, while with increasing rotational frequency, it will change the behavior of MOIs. This is because the ε_6 deformation will change the position of the high-j orbitals and then influence the alignment process of these orbitals in high-spin region [42,62]. Note that the deformation parameter ε_6 is fixed in the present PNC-CSM calculation, while it may change with rotational frequency. I expect that, after considering this effect, the results can be improved further.

The experimental MOIs of even-even Nd and Sm isotopes show that the upbending is weak and becomes less and less obvious with increasing neutron number. To understand this, the occupation probability n_μ of each orbital μ (including both $\alpha = \pm 1/2$) near the Fermi surface for the GSBs in Nd isotopes is shown in Fig. 4. The top and bottom rows are for protons and neutrons, respectively. The positive-parity (negative-parity) levels are denoted by blue solid (red dotted) lines. The Nilsson levels far above the Fermi surface ($n_\mu \sim 0$) and far below ($n_\mu \sim 2$) are not shown. In the PNC-CSM, the total particle number $N = \sum_\mu n_\mu$ is exactly conserved, whereas the occupation probability n_μ for each orbital varies with rotational frequency. By examining the ω dependence of the orbitals near the Fermi surface, one can get some insights into the band crossing. It can be seen from the upper panel of Fig. 4 that, for the proton of ^{152}Nd, the orbitals above the Fermi surface are nearly all empty, and the orbitals below the Fermi surface are nearly all occupied, and they are nearly unchanged with increasing rotational frequency. This is due to the large shell gap at $Z = 60$, which makes the proton

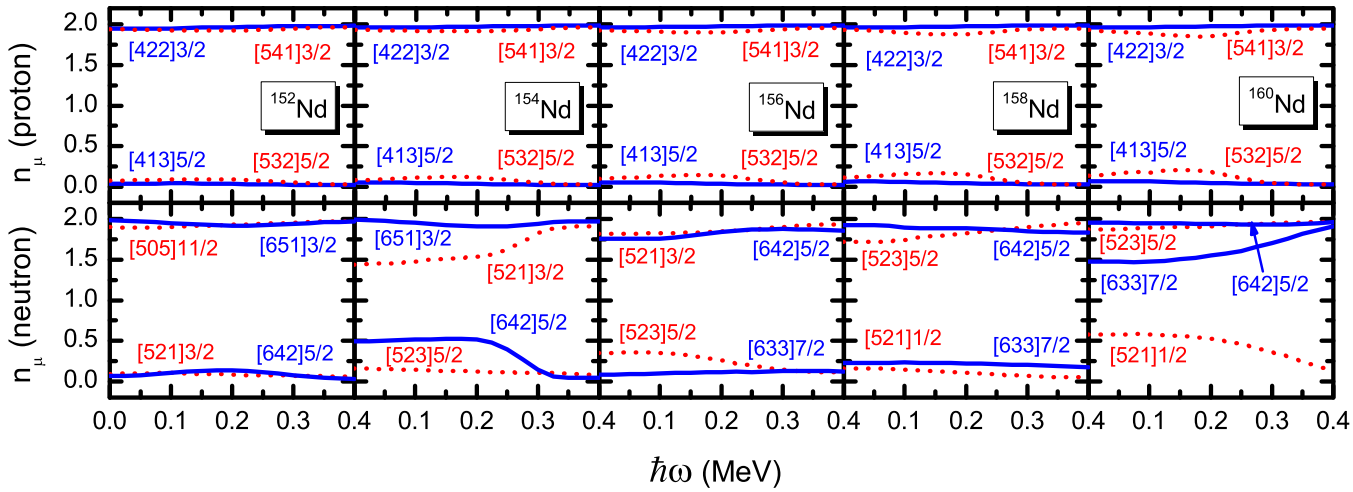

FIG. 4. Occupation probability n_μ of each orbital μ (including both $\alpha = \pm 1/2$) near the Fermi surface for the GSBs in Nd isotopes. The top and bottom rows are for protons and neutrons, respectively. The positive-parity (negative-parity) levels are denoted by blue solid (red dotted) lines. The Nilsson levels far above the Fermi surface ($n_\mu \sim 0$) and far below ($n_\mu \sim 2$) are not shown.

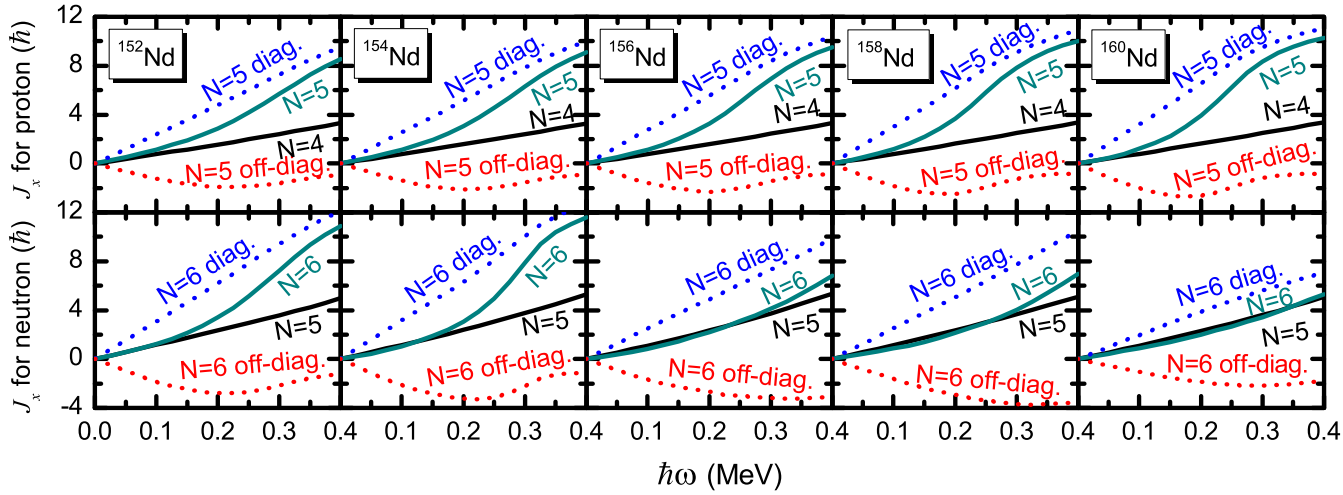

FIG. 5. Contribution of each proton (upper panel) and neutron (lower panel) major shell to the angular-momentum alignment J_x for the GSBs in Nd isotones. The diagonal $\sum_{\mu} j_x(\mu)$ and off-diagonal parts $\sum_{\mu<\nu} j_x(\mu\nu)$ in Eq. (8) from the proton $N = 5$ and neutron $N = 6$ shells are shown by dotted lines.

pairing correlations very weak. With neutron number increasing, especially for ^{160}Nd, $\pi 5/2^-[532]$ and $\pi 3/2^-[541]$ become partly occupied and partly empty, respectively. This is caused by the decreasing of the $Z = 60$ shell gap with increasing neutron number. With rotational frequency increasing, the occupation of $\pi 5/2^-[532]$ and $\pi 3/2^-[541]$ becomes nearly occupied and nearly empty at $\hbar\omega \approx 0.25$ MeV, respectively. Therefore, these two proton $h_{11/2}$ high-j orbitals may contribute to the upbending. It can be seen from the lower panel of Fig. 4 that, for neutrons, only the occupation probabilities of $\nu 5/2^+[642]$ in ^{154}Nd changes drastically around the upbending frequency. Thus, this neutron $i_{13/2}$ orbital may contribute to the upbending in ^{154}Nd. In other Nd isotopes, the occupation probabilities of all the orbitals either remain unchanged or change gradually with increasing rotational frequency. Therefore, the contribution to the upbending from neutrons in these nuclei may be little. The present calculations show that the proton $Z = 62$ shell gap is smaller than the $Z = 60$ shell gap. Therefore, the proton occupation probabilities of Sm isotopes must be a little different from those in Nd isotopes. While for neutrons, the occupation probabilities are very close to each other when the nuclei with the same neutron number is considered. Moreover, it can be seen from Fig. 3 that the behavior of the MOIs for Nd and Sm are quite similar, so only the occupation probabilities for Nd isotopes are given to illustrate the alignment process.

It is well known that the upbending is caused by the alignment of the high-j intruder orbitals [63], which corresponds to the neutron $i_{13/2}$ and proton $h_{11/2}$ orbitals in rare-earth nuclei. To have a clearer understanding of the alignment mechanism in these neutron-rich nuclei, the contribution of each proton and neutron major shell to the total angular-momentum alignment J_x for the GSBs in Nd isotopes is shown in Fig. 5. It can be seen that for proton, the main contribution to the angular-momentum alignment comes from the $N = 5$ major shell ($h_{11/2}$ orbitals). Moreover, the contribution gradually increases with increasing neutron number. While for neutrons, the contribution from the $N = 6$ major shell ($i_{13/2}$ orbitals) is prominent only in ^{152}Nd and ^{154}Nd. In ^{156,158,160}Nd, the contribution from the $N = 6$ major shell gets as small as that from the $N = 5$ major shell. This is due to the fact that, with neutron number increasing, the high-j but high-Ω orbital $\nu 7/2^+[633]$ gets close to the Fermi surface, which contributes not very much to the alignment. Therefore, one can get that difference from a typical nucleus, in which the upbending is caused by whether neutron or proton alignment occurs; both neutron and proton alignments contribute to the upbending in these neutron-rich Nd and Sm isotopes. In the lighter Nd and Sm isotopes, the alignment is due to both neutron $i_{13/2}$ and proton $h_{11/2}$ orbitals. Meanwhile, the proton $h_{11/2}$ orbitals play a more and more important role in the alignment process with neutron number increasing. The competition between the alignment of proton and neutron high-j orbitals makes the upbending in these Nd and Sm isotopes very weak and less obvious with increasing neutron number.

Figure 6 shows the experimental and calculated MOIs of two-qp bands in Nd and Sm isotopes. The experimental MOIs are denoted by full black circles (signature $\alpha = 0$) and open circles (signature $\alpha = 1$), respectively. The MOIs calculated by the PNC-CSM are denoted by black solid lines (signature $\alpha = 0$) and red dotted lines (signature $\alpha = 1$), respectively. The data are taken from Refs. [16,19,21]. It can be seen that the data can be reproduced very well by the PNC-CSM calculations, except two $K^\pi = 5^-$ bands in ^{158}Sm. The agreement between the calculation and the data also supports the configuration assignments for these two-qp states. Note that, in Refs. [16,19], the 1279 keV level is assigned to $\nu^2\, 5/2^-[523] \otimes 5/2^+[642]$ and the 1322 keV level is assigned to $\pi^2 5/2^+[413] \otimes 5/2^-[532]$, respectively. However, the present PNC-CSM calculations show that, if the configuration assignments for these two bands are changed, the MOIs can be reproduced quite well. In addition, as I mentioned before, the 1398 keV state in ^{156}Sm was previously assigned to $K^\pi = 5^-$ in Ref. [16]. It can be seen that the calculated MOIs for this band with $K^\pi = 4^-$ and 5^- configurations are similar. Therefore, it is difficult to distinguish

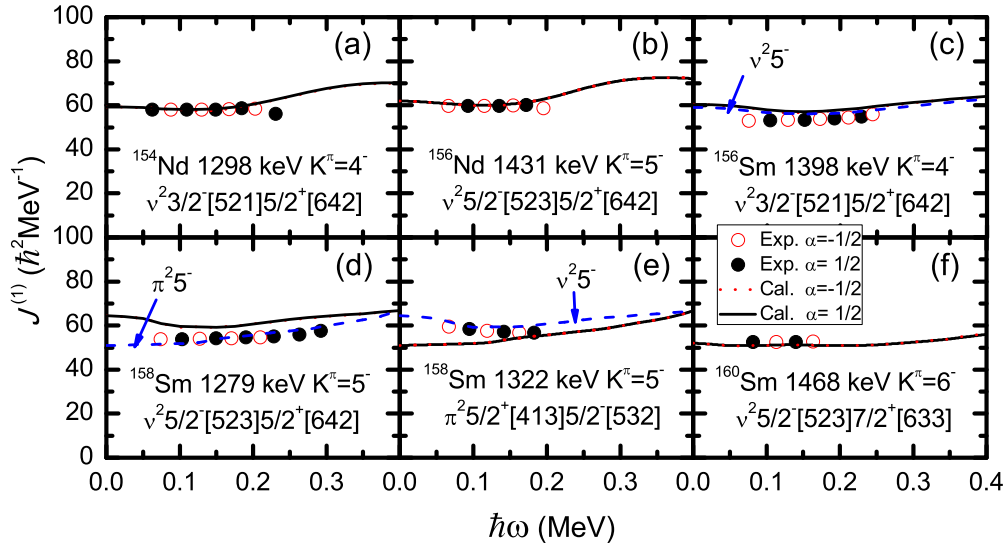

FIG. 6. The experimental and calculated MOIs of two-qp bands in Nd and Sm isotopes. The experimental MOIs are denoted by full black circles (signature $\alpha = 0$) and open circles (signature $\alpha = 1$), respectively. The calculated MOIs by the PNC-CSM are denoted by black solid lines (signature $\alpha = 0$) and red dotted lines (signature $\alpha = 1$), respectively. The data are taken from Refs. [16,19,21]. $\nu^2 5^-$ and $\pi^2 5^-$ denote $\nu^2 5/2^-[523] \otimes 5/2^+[642]$ and $\pi^2 5/2^+[413] \otimes 5/2^-[532]$, respectively.

these two configuration assignments by their MOIs. Due to the fact that the calculated excitation energy of $K^\pi = 4^-$ is very close to the data, this state is attentively assigned as $K^\pi = 4^-$. More detailed experimental information is needed to give a solid configuration assignment for this state.

Except for even-even Nd and Sm isotopes, some one-qp rotational bands, including both the ground- and excited-state bands, have been identified in the odd-A nuclei, which can provide more detailed information on the single-particle structure for these neutron-rich nuclei. Figure 7 shows the experimental and calculated kinematic MOIs $J^{(1)}$ of the GSBs for odd-A Nd and Sm isotopes. The available data are taken from Refs. [17,58,59]. The experimental MOIs are denoted by full squares (signature $\alpha = +1/2$) and open squares (signature $\alpha = -1/2$), respectively. The MOIs calculated by the PNC method are denoted by solid lines (signature $\alpha = +1/2$) and dotted lines (signature $\alpha = -1/2$), respectively. The experimental data show that the ground states of $N = 153$ (^{153}Nd and ^{155}Sm) and $N = 157$ (^{157}Nd and ^{159}Sm) isotones

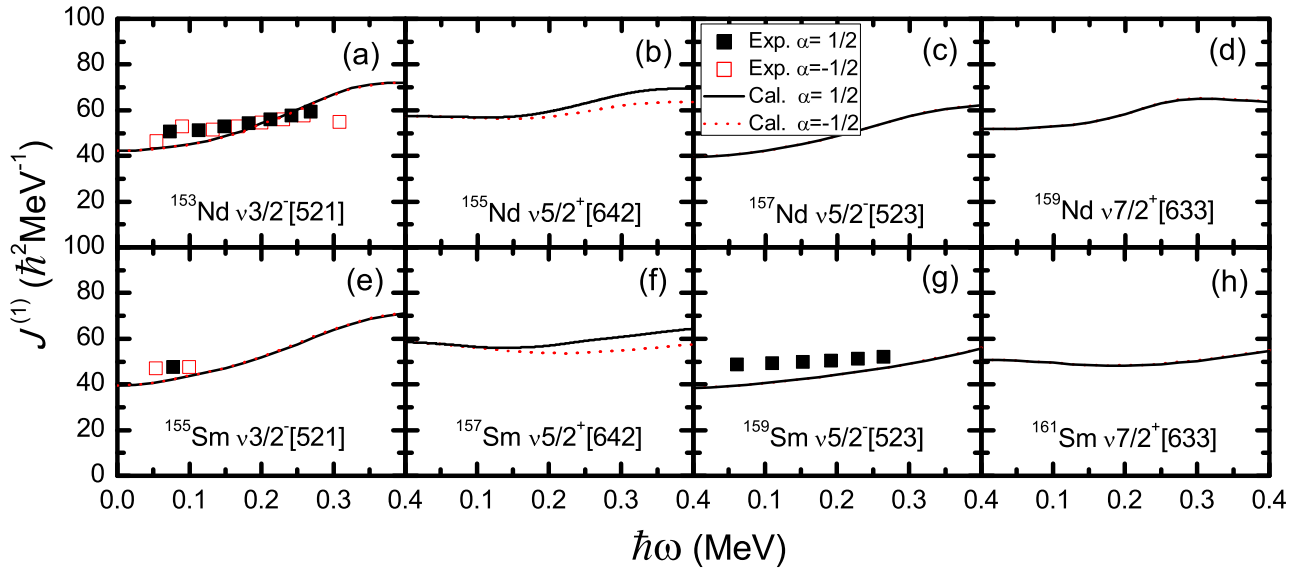

FIG. 7. The experimental and calculated kinematic MOIs $J^{(1)}$ of the GSBs for odd-A Nd and Sm isotopes. The data are taken from Refs. [17,58,59]. The experimental MOIs are denoted by full squares (signature $\alpha = +1/2$) and open squares (signature $\alpha = -1/2$), respectively. The MOIs calculated by the PNC-CSM are denoted by solid lines (signature $\alpha = +1/2$) and dotted lines (signature $\alpha = -1/2$), respectively.

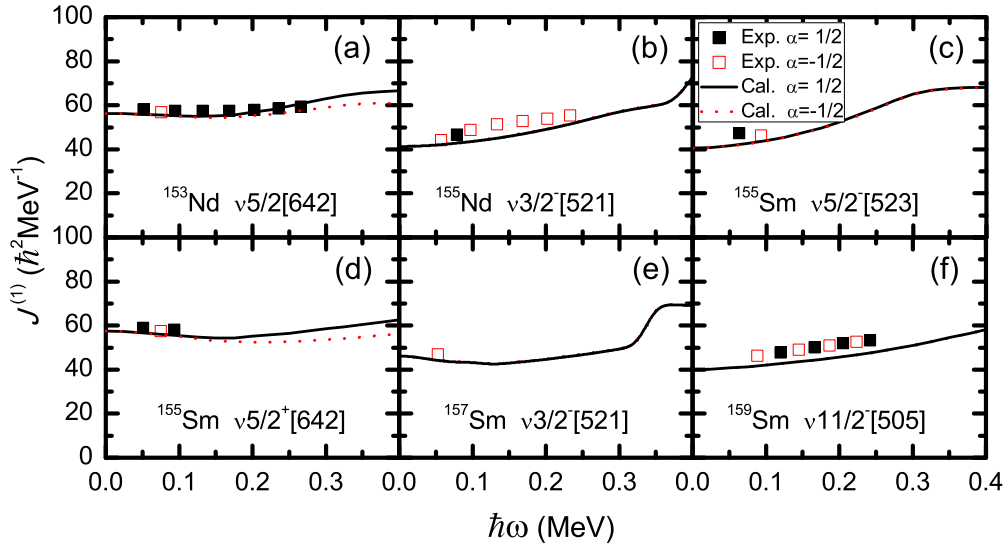

FIG. 8. Similar as Fig. 7, but for the excited one-qp bands in odd-A Nd and Sm isotopes. The data are taken from Refs. [14,17,18,59].

are $\nu 3/2^-[521]$ and $\nu 5/2^-[523]$, respectively. The present calculations are also consistent with the data. Therefore, from the cranked Nilsson levels in Fig. 2 one can get that the ground state of $N = 155$ isotones should be $\nu^- 5/2[642]$. However, in Ref. [14] the data show that the ground state of ^{155}Nd is $\nu 3/2^-[521]$, which is different from the PNC-CSM calculation. From a systematic point of view, I put the $\nu^- 5/2[642]$ as the ground state of $N = 155$ isotones. Similar to Fig. 7, the MOIs for the one-qp excited bands are shown in Fig. 8. The data are taken from Refs. [14,17,18,59]. It can be seen from Figs. 7 and 8 that the MOIs of these rotational bands in odd-A Nd and Sm isotopes can be well reproduced by the PNC-CSM, which in turn confirms the configuration assignments for these one-qp states.

V. SUMMARY

In summary, the rotational properties of the neutron-rich Nd and Sm isotopes with mass number $A \approx 150$ are investigated by using the cranked shell model with pairing correlations treated by a particle-number conserving method, in which the Pauli blocking effects are taken into account exactly. The excitation energies of several experimentally observed two-qp K isomers are reproduced quite well by the PNC-CSM calculation. Furthermore, all two-qp states in even-even Nd and Sm isotopes with excitation energies lower than 2.5 MeV are systematically calculated, and possible four-qp K isomers with the lowest two-quasi-proton and two-quasi-neutron configurations are predicted. Moreover, the experimentally observed rotational frequency variations of MOIs for the even-even and odd-A nuclei are reproduced very well by the PNC-CSM calculations. The effects of high-order deformation ε_6 on the two-qp excitation energies and MOIs of the GSBs are analyzed. By analyzing the occupation probability n_μ of each cranked Nilsson orbitals near the Fermi surface and the contribution of each major shell to the angular-momentum alignments, the alignment mechanism in these nuclei is understood clearly.

ACKNOWLEDGMENTS

Helpful discussions with Shan–Gui Zhou are gratefully acknowledged. This work was partly supported by the National Natural Science Foundation of China (Grants No. 11505058, No. 11775112, and No. 11775026), and the Fundamental Research Funds for the Central Universities (2018MS058).

[1] F. Iachello and N. V. Zamfir, Phys. Rev. Lett. **92**, 212501 (2004).
[2] T. Nikšić, D. Vretenar, G. A. Lalazissis, and P. Ring, Phys. Rev. Lett. **99**, 092502 (2007).
[3] W. R. Phillips, I. Ahmad, H. Emling, R. Holzmann, R. V. F. Janssens, T. L. Khoo, and M. W. Drigert, Phys. Rev. Lett. **57**, 3257 (1986).
[4] W. R. Phillips, R. V. F. Janssens, I. Ahmad, H. Emling, R. Holzmann, T. L. Khoo, and M. W. Drigert, Phys. Lett. B **212**, 402 (1988).
[5] R. Ibbotson, C. A. White, T. Czosnyka, P. A. Butler, N. Clarkson, D. Cline, R. A. Cunningham, M. Devlin, K. G. Helmer, T. H. Hoare, J. R. Hughes, G. D. Jones, A. E. Kavka, B. Kotlinski, R. J. Poynter, P. Regan, E. G. Vogt, R. Wadsworth, D. L. Watson, and C. Y. Wu, Phys. Rev. Lett. **71**, 1990 (1993).
[6] P. Walker and G. Dracoulis, Nature (London) **399**, 35 (1999).
[7] R. C. Greenwood, R. A. Anderl, J. D. Cole, and H. Willmes, Phys. Rev. C **35**, 1965 (1987).

[8] J. H. Hamilton, A. V. Ramayya, S. J. Zhu, G. M. Ter-Akopian, Y. T. Oganessian, J. D. Cole, J. O. Rasmussen, and M. A. Stoyer, Prog. Part. Nucl. Phys. **35**, 635 (1995).

[9] J. H. Hamilton, A. V. Ramayya, J. K. Hwang, J. Kormicki, B. R. S. Babu, A. Sandulescu, A. Florescu, W. Greiner, G. M. Ter-Akopian, Y. T. Oganessian, A. V. Daniel, S. J. Zhu, M. G. Wang, T. Ginter, J. K. Deng, W. C. Ma, G. S. Popeko, Q. H. Lu, E. Jones, R. Dodder, P. Gore, W. Nazarewicz, J. O. Rasmussen, S. Asztalos, I. Y. Lee, S. Y. Chu, K. E. Gregorich, A. O. Macchiavelli, M. F. Mohar, S. Prussin, M. A. Stoyer, R. W. Lougheed, K. J. Moody, J. F. Wild, L. A. Bernstein, J. A. Becker, J. D. Cole, R. Aryaeinejad, Y. X. Dardenne, M. W. Drigert, K. Butler-Moore, R. Donangelo, and H. C. Griffin, Prog. Part. Nucl. Phys. **38**, 273 (1997).

[10] S. J. Zhu, J. H. Hamilton, A. V. Ramayya, B. R. S. Babu, Q. H. Lu, W. C. Ma, T. N. Ginter, M. G. Wang, J. Kormicki, J. K. Deng, D. Shi, J. D. Cole, R. Aryaeinejad, J. Rasmussen, M. A. Stoyer, S. Y. Chu, K. Gregorich, M. F. Mohar, S. Prussin, G. M. Ter-Akopian, Y. T. Oganessian, N. R. Johnson, I. Y. Lee, and F. K. McGowan, J. Phys. G **21**, L57 (1995).

[11] B. R. S. Babu, S. J. Zhu, A. V. Ramayya, J. H. Hamilton, L. K. Peker, M. G. Wang, T. N. Ginter, J. Kormicki, W. C. Ma, J. D. Cole, R. Aryaeinejad, K. Butler-Moore, Y. X. Dardenne, M. W. Drigert, G. M. Ter-Akopian, Y. T. Oganessian, J. O. Rasmussen, S. Asztalos, I. Y. Lee, A. O. Macchiavelli, S. Y. Chu, K. E. Gregorich, M. F. Mohar, S. Prussin, M. A. Stoyer, R. W. Lougheed, K. J. Moody, and J. F. Wild, Phys. Rev. C **54**, 568 (1996).

[12] X. Q. Zhang, J. H. Hamilton, A. V. Ramayya, L. K. Peker, J. K. Hwang, E. F. Jones, J. Komicki, C. J. Beyer, P. M. Gore, B. R. S. Babu, T. N. Ginter, S. J. Asztalos, S. Y. Chu, K. E. Gregorich, I. Y. Lee, A. O. Macchiavelli, R. W. Macleod, J. O. Rasmussen, J. Gilat, G. M. Ter-Akopian, Y. T. Oganessian, A. V. Daniel, W. C. Ma, P. G. Varmette, J. D. Cole, R. Aryaeinejad, K. Butler-Moore, Y. X. Dardenne, M. W. Drigert, M. A. Stoyer, J. F. Wild, J. A. Becker, L. A. Bernstein, R. W. Lougheed, K. J. Moody, R. Donangelo, S. G. Prussin, and H. C. Griffin, Phys. Rev. C **57**, 2040 (1998).

[13] C. Gautherin, M. Houry, W. Korten, Y. Le Coz, R. Lucas, X. Phan, C. Theisen, C. Badimon, G. Barreau, T. Doan, G. Pedemay, G. Bélier, M. Girod, V. Méot, S. Peru, A. Astier, L. Ducroux, M. Meyer, and N. Redon, Eur. Phys. J. A **1**, 391 (1998).

[14] J. K. Hwang, A. V. Ramayya, J. H. Hamilton, K. Li, C. Goodin, Y. X. Luo, J. O. Rasmussen, and S. J. Zhu, Phys. Rev. C **78**, 014309 (2008).

[15] J. K. Hwang, A. V. Ramayya, J. H. Hamilton, K. Li, C. Goodin, Y. X. Luo, J. O. Rasmussen, and S. J. Zhu, Phys. Rev. C **78**, 017303 (2008).

[16] G. S. Simpson, W. Urban, J. Genevey, R. Orlandi, J. A. Pinston, A. Scherillo, A. G. Smith, J. F. Smith, I. Ahmad, and J. P. Greene, Phys. Rev. C **80**, 024304 (2009).

[17] W. Urban, J. A. Pinston, G. S. Simpson, A. G. Smith, J. F. Smith, T. Rzaca-Urban, and I. Ahmad, Phys. Rev. C **80**, 037301 (2009).

[18] J. K. Hwang, A. V. Ramayya, J. H. Hamilton, S. H. Liu, N. T. Brewer, Y. X. Luo, J. O. Rasmussen, S. J. Zhu, and R. Donangelo, Phys. Rev. C **82**, 034308 (2010).

[19] E. H. Wang, J. H. Hamilton, A. V. Ramayya, J. K. Hwang, S. H. Liu, N. T. Brewer, Y. X. Luo, J. O. Rasmussen, S. J. Zhu, G. M. Ter-Akopian, and Y. T. Oganessian, Phys. Rev. C **90**, 067306 (2014).

[20] Z. Patel, P.-A. Söderström, Z. Podolyák, P. H. Regan, P. M. Walker, H. Watanabe, E. Ideguchi, G. S. Simpson, H. L. Liu, S. Nishimura, Q. Wu, F. R. Xu, F. Browne, P. Doornenbal, G. Lorusso, S. Rice, L. Sinclair, T. Sumikama, J. Wu, Z. Y. Xu, N. Aoi, H. Baba, F. L. Bello Garrote, G. Benzoni, R. Daido, Y. Fang, N. Fukuda, G. Gey, S. Go, A. Gottardo, N. Inabe, T. Isobe, D. Kameda, K. Kobayashi, M. Kobayashi, T. Komatsubara, I. Kojouharov, T. Kubo, N. Kurz, I. Kuti, Z. Li, M. Matsushita, S. Michimasa, C.-B. Moon, H. Nishibata, I. Nishizuka, A. Odahara, E. Şahin, H. Sakurai, H. Schaffner, H. Suzuki, H. Takeda, M. Tanaka, J. Taprogge, Z. Vajta, A. Yagi, and R. Yokoyama, Phys. Rev. Lett. **113**, 262502 (2014).

[21] Z. Patel, Z. Podolyák, P. M. Walker, P. H. Regan, P.-A. Söderström, H. Watanabe, E. Ideguchi, G. S. Simpson, S. Nishimura, F. Browne, P. Doornenbal, G. Lorusso, S. Rice, L. Sinclair, T. Sumikama, J. Wu, Z. Y. Xu, N. Aoi, H. Baba, F. L. Bello Garrote, G. Benzoni, R. Daido, Z. Dombrádi, Y. Fang, N. Fukuda, G. Gey, S. Go, A. Gottardo, N. Inabe, T. Isobe, D. Kameda, K. Kobayashi, M. Kobayashi, T. Komatsubara, I. Kojouharov, T. Kubo, N. Kurz, I. Kuti, Z. Li, H. L. Liu, M. Matsushita, S. Michimasa, C.-B. Moon, H. Nishibata, I. Nishizuka, A. Odahara, E. Şahin, H. Sakurai, H. Schaffner, H. Suzuki, H. Takeda, M. Tanaka, J. Taprogge, Z. Vajta, F. R. Xu, A. Yagi, and R. Yokoyama, Phys. Lett. B **753**, 182 (2016).

[22] E. Ideguchi, G. S. Simpson, R. Yokoyama, M. Tanaka, S. Nishimura, P. Doornenbal, G. Lorusso, P.-A. Söderström, T. Sumikama, J. Wu, Z. Y. Xu, N. Aoi, H. Baba, F. L. Bello Garrote, G. Benzoni, F. Browne, R. Daido, Y. Fang, N. Fukuda, A. Gottardo, G. Gey, S. Go, N. Inabe, T. Isobe, D. Kameda, K. Kobayashi, M. Kobayashi, I. Kojouharov, T. Komatsubara, T. Kubo, N. Kurz, I. Kuti, Z. Li, M. Matsushita, S. Michimasa, C.-B. Moon, H. Nishibata, I. Nishizuka, A. Odahara, Z. Patel, S. Rice, E. Sahin, H. Sakurai, H. Schaffner, L. Sinclair, H. Suzuki, H. Takeda, J. Taprogge, Z. Vajta, H. Watanabe, and A. Yagi, Phys. Rev. C **94**, 064322 (2016).

[23] Y.-C. Yang, Y. Sun, S.-J. Zhu, M. Guidry, and C.-L. Wu, J. Phys. G **37**, 085110 (2010).

[24] Y. C. Yang and Y. Sun, Sci. China-Phys. Mech. Astron. (Suppl. 1) **54**, 81 (2011).

[25] J. Y. Zeng and T. S. Cheng, Nucl. Phys. A **405**, 1 (1983).

[26] J. Y. Zeng, T. H. Jin, and Z. J. Zhao, Phys. Rev. C **50**, 1388 (1994).

[27] C. S. Wu and J. Y. Zeng, Phys. Rev. C **39**, 666 (1989).

[28] J. Y. Zeng, Y. A. Lei, T. H. Jin, and Z. J. Zhao, Phys. Rev. C **50**, 746 (1994).

[29] S. X. Liu, J. Y. Zeng, and E. G. Zhao, Phys. Rev. C **66**, 024320 (2002).

[30] X. T. He, S. X. Liu, S. Y. Yu, J. Y. Zeng, and E. G. Zhao, Eur. Phys. J. A **23**, 217 (2005).

[31] X. Wu, Z. H. Zhang, J. Y. Zeng, and Y. A. Lei, Phys. Rev. C **83**, 034323 (2011).

[32] Z.-H. Zhang, P.-W. Zhao, J. Meng, J.-Y. Zeng, E.-G. Zhao, and S.-G. Zhou, Phys. Rev. C **87**, 054314 (2013).

[33] Z.-H. Zhang, Phys. Rev. C **94**, 034305 (2016).

[34] S. X. Liu, J. Y. Zeng, and L. Yu, Nucl. Phys. A **735**, 77 (2004).

[35] Z. H. Zhang, X. Wu, Y. A. Lei, and J. Y. Zeng, Nucl. Phys. A **816**, 19 (2009).

[36] Z. H. Zhang, Y. A. Lei, and J. Y. Zeng, Phys. Rev. C **80**, 034313 (2009).

[37] Z.-H. Zhang, Sci. China: Phys., Mech. Astron. **59**, 672012 (2016).
[38] Z.-H. Zhang, Nucl. Phys. A **949**, 22 (2016).
[39] X. T. He, Z. Z. Ren, S. X. Liu, and E. G. Zhao, Nucl. Phys. A **817**, 45 (2009).
[40] Z.-H. Zhang, J.-Y. Zeng, E.-G. Zhao, and S.-G. Zhou, Phys. Rev. C **83**, 011304R (2011).
[41] Z.-H. Zhang, X.-T. He, J.-Y. Zeng, E.-G. Zhao, and S.-G. Zhou, Phys. Rev. C **85**, 014324 (2012).
[42] Z.-H. Zhang, J. Meng, E.-G. Zhao, and S.-G. Zhou, Phys. Rev. C **87**, 054308 (2013).
[43] J. Meng, J.-Y. Guo, L. Liu, and S.-Q. Zhang, Front. Phys. Chin. **1**, 38 (2006).
[44] N. Pillet, P. Quentin, and J. Libert, Nucl. Phys. A **697**, 141 (2002).
[45] W. Y. Liang, C. F. Jiao, Q. Wu, X. M. Fu, and F. R. Xu, Phys. Rev. C **92**, 064325 (2015).
[46] X. M. Fu, F. R. Xu, J. C. Pei, C. F. Jiao, Y. Shi, Z. H. Zhang, and Y. A. Lei, Phys. Rev. C **87**, 044319 (2013).
[47] X. Fu, C. Jiao, F. Xu, and Z. Zhang, Sci. China: Phys., Mech. Astron. **56**, 1423 (2013).
[48] Z. Shi, Z. H. Zhang, Q. B. Chen, S. Q. Zhang, and J. Meng, Phys. Rev. C **97**, 034317 (2018).
[49] R. W. Richardson and N. Sherman, Nucl. Phys. **52**, 221 (1964).
[50] F. Pan, J. P. Draayer, and W. E. Ormand, Phys. Lett. B **422**, 1 (1998).
[51] A. Volya, B. A. Brown, and V. Zelevinsky, Phys. Lett. B **509**, 37 (2001).
[52] L. Y. Jia, Phys. Rev. C **88**, 044303 (2013).
[53] L. Y. Jia, Phys. Rev. C **88**, 064321 (2013).
[54] W.-C. Chen, J. Piekarewicz, and A. Volya, Phys. Rev. C **89**, 014321 (2014).
[55] S. G. Nilsson, C. F. Tsang, A. Sobiczewski, Z. Szymaski, S. Wycech, C. Gustafson, I. L. Lamm, P. Möller, and B. Nilsson, Nucl. Phys. A **131**, 1 (1969).
[56] H. Molique and J. Dudek, Phys. Rev. C **56**, 1795 (1997).
[57] P. Möller, J. R. Nix, W. D. Myers, and W. J. Swiatecki, At. Data Nucl. Data Tables **59**, 185 (1995).
[58] J. K. Hwang, A. V. Ramayya, J. H. Hamilton, J. Kormicki, L. K. Peker, B. R. S. Babu, T. N. Ginter, G. M. Ter-Akopian, Y. T. Oganessian, A. V. Daniel, W. C. Ma, P. G. Varmette, S. J. Asztalos, S. Y. Chu, K. E. Gregorich, I. Y. Lee, A. O. Macchiavelli, R. W. Macleod, J. O. Rasmussen, J. D. Cole, R. Aryaeinejad, K. Butler-Moore, Y. X. Dardenne, M. W. Drigert, M. A. Stoyer, J. F. Wild, J. A. Becker, L. A. Bernstein, R. W. Lougheed, K. J. Moody, R. Donangelo, S. G. Prussin, and H. C. Griffin, Int. J. Mod. Phys. E **06**, 331 (1997).
[59] C. W. Reich, Nucl. Data Sheets **104**, 1 (2005).
[60] M. Wang, G. Audi, A. H. Wapstra, F. G. Kondev, M. MacCormick, X. Xu, and B. Pfeiffer, Chin. Phys. C **36**, 1603 (2012).
[61] M. Diebel, Nucl. Phys. A **419**, 221 (1984).
[62] H. L. Liu, F. R. Xu, and P. M. Walker, Phys. Rev. C **86**, 011301R (2012).
[63] F. S. Stephens and R. S. Simon, Nucl. Phys. A **183**, 257 (1972).